Topological chiral spin liquids and competing states in triangular lattice SU(N) Mott insulators

Xu-Ping Yao [1], Yonghao Gao,[2] and Gang Chen [1,*]

[1]*Department of Physics and HKU-UCAS Joint Institute for Theoretical and Computational Physics at Hong Kong, University of Hong Kong, Pokfulam Road, Hong Kong, China*

[2]*State Key Laboratory of Surface Physics and Department of Physics, Fudan University, Shanghai 200433, China*

(Received 5 December 2020; revised 27 March 2021; accepted 27 April 2021; published 21 May 2021)

SU(N) Mott insulators have been proposed and/or realized in solid-state materials and with ultracold atoms on optical lattices. We study the two-dimensional SU(N) antiferromagnets on the triangular lattice. Starting from an SU(N) Heisenberg model with the fundamental representation on each site in the large-N limit, we perform a self-consistent calculation and find a variety of ground states including the valence cluster states, stripe ordered states with a doubled unit cell, and topological chiral spin liquids. The system favors a cluster or ordered ground state when the number of flavors N is less than 6. It is shown that increasing the number of flavors enhances quantum fluctuations and eventually transfers the clusterized ground states into topological chiral spin liquids. This chiral spin liquid ground state has an equivalent for the square lattice SU(N) magnets. We further identify the corresponding lowest competing states that represent another distinct type of chiral spin liquid state. We conclude with a discussion of the relevant systems and the experimental probes.

DOI: 10.1103/PhysRevResearch.3.023138

I. INTRODUCTION

SU(N) Mott insulators are representative examples of quantum systems with a large local Hilbert space where quantum fluctuations can be strongly enhanced and exotic quantum phases could be stabilized. All the SU(N) spin operators are present in the effective model for the Mott insulators and would be able to shuffle all the spin states rather actively in the local Hilbert space. The system can be quite delocalized within the local Hilbert space, that is, to enhance quantum fluctuations and induce exotic quantum phases. This aspect is fundamentally different from the SU(2) Mott insulators with large-S local moments that also have a large local Hilbert space. For the large-S SU(2) Mott insulators, the pairwise Heisenberg interaction is quite ineffective in delocalizing the spin states in the large-S Hilbert space, and thus quantum fluctuations are strongly suppressed. Thus, it is the conventional wisdom not to search for exotic quantum phases among the large-S SU(2) Mott insulators, but among the spin-1/2 quantum magnets with a strong frustration. In contrast, the emergence of the SU(N) Mott insulators brings a new searching direction for exotic quantum phases.

SU(N) Mott insulators are not a theoretical fantasy, but exist in nature. It has been shown that the ultracold alkaline-earth atoms (AEAs) on optical lattices can simulate quantum many-body physics with an SU(N) symmetry without any fine-tuning [1]. The nuclear spin of fermionic AEAs can be as large as $I = 9/2$ for ^{87}Sr, while the outer shell electrons give a total spin $S = 0$ and make the hyperfine coupling inactive. This observation effectively extends the realization of SU(N) magnets up to $N = 2I + 1$. Early efforts by Wu explored total spin-3/2 alkaline fermions on optical lattices where the SU(4) symmetry can be achieved with fine-tuning [2–5]. Quantum Monte Carlo simulations were introduced later to study magnetic properties of the SU($2N$) Hubbard model [6,7]. There is also some effort in searching for an emergent SU(N) symmetry in real materials particularly for the SU(4) case. The two-orbital Kugel-Khomskii model can become SU(4) symmetric after some fine-tuning [8,9]. Experimental and numerical evidence also suggests that $Ba_3CuSb_2O_9$ could be a prominent candidate on a decorated honeycomb lattice [10], though the Cu-Sb dumbbell is quenched rather than an active degree of freedom. The SU(4) Heisenberg model has further been proposed for the spin-orbit-coupled Mott insulator α-$ZrCl_3$ where the degree of freedom is the spin-orbit-entangled $J = 3/2$ local moment [11] on a honeycomb lattice [12]. More recently, it has been proposed that the Mott-insulating and superconducting behaviors in twisted bilayer graphenes can be captured by a two-orbital Hubbard model with an emergent SU(4) symmetry on a moiré triangular lattice [13]. Other work even suggested that double moiré layers, built from transition metal dichalcogenides or graphenes, separated from one another by a thin insulating layer, would be a natural platform to realize Hubbard models on the triangular lattice with SU(4) or SU(8) symmetries [14,15].

Owing to enhanced quantum fluctuations for SU(N) Mott insulators, the pioneering theoretical works [16,17] by Hermele *et al.* have obtained the topological chiral spin liquid (CSL) ground states with intrinsic topological orders even for an unfrustrated square lattice when $N \geqslant 5$ [16–18].

*gangchen@hku.hk

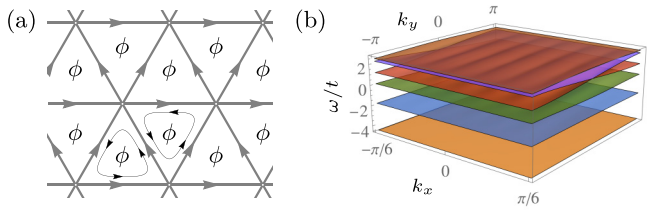

FIG. 1. (a) Triangular lattice with background U(1) gauge flux ϕ within each plaquette. (b) The spinon dispersions for chiral spin liquids with $\phi = 5\pi/6$.

Depending on the atom occupation numbers, the system can support both Abelian and non-Abelian statistics for the anyonic excitations. Since unfrustrated lattices such as square and honeycomb lattices already bring exotic and interesting physics [19–21], the frustrated lattices could further harbor nontrivial quantum phases, for example the triangular lattice with SU(3) and SU(4) spins [22–24]. In this work, we focus on the SU(N) Heisenberg model on a triangular lattice where each lattice site comprises the fundamental representation of the SU(N) group. For AEAs, this corresponds to one atom per lattice site and is known to be most stable against the three-body loss. Because the $1/N$ filling is kept throughout, the large-N limit differs fundamentally from the large-N extension of the spin-1/2 SU(2) models where the 1/2 is kept and two sites can form a SU(2) spin singlet [25]. Here, as N sites are needed to form a singlet, the valence cluster solid (VCS) state is generically disfavored in the large-N limit. Instead, by our large-N calculation, two types of CSL states with background U(1) gauge flux $\phi = \pi - \pi/N$ and $\pi - \pi/(2N)$ [see Fig. 1(a)] are identified as the ground and lowest competing states for $6 \leqslant N \leqslant 9$, respectively. For smaller N's, various symmery-broken cluster or stripe states are obtained. We expect the large-N results are more reliable when N is large.

The rest of this paper is organized as follows. The general Heisenberg model of SU(N) spins is introduced and simplified at the large-N saddle point in Sec. II. The self-consistent minimization algorithm is implemented to solve the reduced mean-field spinon Hamiltonian. The technique details of this algorithm are described in Sec. III. It is emphasized that the optimized solutions strictly satisfy the local constraints. In Sec. IV, both the ground states and lowest competing states for $2 \leqslant N \leqslant 9$ are reported and analyzed, especially for two types of CSL states. Finally, in Sec. V, this work concludes with a discussion of relevant systems and the experimental probes.

II. THE SU(N) HEISENBERG MODEL IN THE LARGE-N APPROXIMATION

We begin with an SU(N) Heisenberg model on the triangular lattice where each site comprises the fundamental representation of the SU(N) group. This model can be obtained from the strong-coupling limit of an SU(N) Hubbard model with $1/N$ filling or one particle per site. The SU(N) Heisenberg model is given as

$$\mathcal{H} = J \sum_{\langle \boldsymbol{r}\boldsymbol{r}' \rangle} S_{\alpha\beta}(\boldsymbol{r}) S_{\beta\alpha}(\boldsymbol{r}'), \tag{1}$$

where J is the antiferromagnetic exchange interaction and the sum is taken over the nearest-neighbor bonds and spin flavors. The SU(N) spin operators can be simply expressed with the Abrikosov fermion representation $S_{\alpha\beta}(\boldsymbol{r}) = f^\dagger_{\boldsymbol{r}\alpha} f_{\boldsymbol{r}\beta}$, and $\alpha, \beta = 1, \ldots, N$. Hereafter, a summation over repeated indices in the form of Greek letters is supposed unless otherwise specified. A local constraint on the fermion occupation $f^\dagger_{\boldsymbol{r}\alpha} f_{\boldsymbol{r}\alpha} = 1$ is imposed to reduce the enlarged Hilbert space. In principle, an SU(N) singlet could be formed by N sites. But the SU(N) exchange rapidly transforms one N-site singlet to other sets of N-site singlets, resulting in a failure of the conventional understanding. Instead, the spin Hamiltonian Eq. (1) is solvable in the limit $N \to \infty$ via a large-N saddle point approximation in the imaginary-time path integral formulation. The corresponding partition function can be expressed as

$$\mathcal{Z} = \int \mathcal{D}\chi^\dagger \mathcal{D}\chi \mathcal{D}\mu \mathcal{D}f^\dagger \mathcal{D}f e^{-\mathcal{S}}. \tag{2}$$

The action $\mathcal{S}$ is given as

$$\mathcal{S} = \int_0^\beta d\tau \left[\sum_{\boldsymbol{r}} f^\dagger_{\boldsymbol{r}\alpha} \partial_\tau f_{\boldsymbol{r}\alpha} + \sum_{\langle \boldsymbol{r}\boldsymbol{r}' \rangle} (\chi_{\boldsymbol{r}\boldsymbol{r}'} f^\dagger_{\boldsymbol{r}\alpha} f_{\boldsymbol{r}'\alpha} + \text{H.c.}) + N \sum_{\langle \boldsymbol{r}\boldsymbol{r}' \rangle} \frac{|\chi_{\boldsymbol{r}\boldsymbol{r}'}|^2}{\mathcal{J}} + \sum_{\boldsymbol{r}} \mu_{\boldsymbol{r}} (f^\dagger_{\boldsymbol{r}\alpha} f_{\boldsymbol{r}\alpha} - 1) \right], \tag{3}$$

where $\mu_{\boldsymbol{r}}$ is the Lagrangian multiplier to enforce the Hilbert space constraint, $\chi_{\boldsymbol{r}\boldsymbol{r}'}$ is the auxiliary field to decouple the fermion operators, and $\mathcal{J} \equiv NJ$. As the action $\mathcal{S}$ scales linearly with N, the large-N limit leads to a saddle point approximation that results in the saddle point equations, $\chi_{\boldsymbol{r}\boldsymbol{r}'} = -\mathcal{J}\langle f^\dagger_{\boldsymbol{r}'\alpha} f_{\boldsymbol{r}\alpha} \rangle / N$, $\langle f^\dagger_{\boldsymbol{r}\alpha} f_{\boldsymbol{r}\alpha} \rangle = 1$, and the saddle point or mean-field Hamiltonian for the fermionic spinons is

$$\mathcal{H}_{\text{MF}} = \frac{N}{\mathcal{J}} \sum_{\langle \boldsymbol{r}\boldsymbol{r}' \rangle} |\chi_{\boldsymbol{r}\boldsymbol{r}'}|^2 + \sum_{\langle \boldsymbol{r}\boldsymbol{r}' \rangle} (\chi_{\boldsymbol{r}\boldsymbol{r}'} f^\dagger_{\boldsymbol{r}\alpha} f_{\boldsymbol{r}'\alpha} + \text{H.c.}) + \sum_{\boldsymbol{r}} \mu_{\boldsymbol{r}} (1 - f^\dagger_{\boldsymbol{r}\alpha} f_{\boldsymbol{r}\alpha}). \tag{4}$$

In the following, we will search for the saddle point with the lowest mean-field energy E_{MF} numerically and discuss the properties of ground states. Before that, we first discuss the lower bound of E_{MF} and the bound saturation conditions for reference. An exact lower bound on E_{MF} for generic lattices [26] was first obtained by Rokhsar for the half filling, and was shown to be saturated by valence bond states with various spin singlet coverings. These states break the lattice translation but

preserve the spin-rotation symmetry, and fluctuations beyond the mean field can break the high degeneracy among them [25]. The lower bound was generalized to the $1/N$ filling with [17]

$$E_{\mathrm{MF}} \geqslant -N_s \frac{N-1}{2N} \mathcal{J}_{\max}, \tag{5}$$

where N_s is the number of lattice sites.

We set $\mathcal{J}_{\max} = \mathcal{J}$ for each bond. The saturation for Eq. (5) is reached by an N-simplex VCS state composed by N-site simplices. That is, every site on the lattice is directly connected to the other $N-1$ sites within the same cluster by a single bond with an exchange coupling $\mathcal{J}_{\max}$. On a d-dimensional lattice, the N-simplex VCS with $N > d+1$ is prohibited without fine-tuning of the exchange. Thus, there are only two-simplex and three-simplex VCSs on the triangular lattice. For $N \geqslant 4$, possible cluster states are general N-site ones satisfying a stricter energy bound [17] $E_{\mathrm{MF}} \geqslant -\mathcal{N}_b \mathcal{J}_{\max}/N$, where $\mathcal{N}_b$ is the total number of isolated bonds in the lattice.

III. THE SCM ALGORITHM

To determine the saddle point solutions, we closely follow the numerical self-consistent minimization (SCM) algorithm developed in Refs. [16,17]. The technical details of the algorithm are described in the following. During one energy optimization process for a given geometry and periodic boundary conditions, the algorithm starts from initializing the fields $\chi_{\boldsymbol{r}\boldsymbol{r}'}$ at each bond randomly with $\chi_{\boldsymbol{r}\boldsymbol{r}'} = |\chi_{\boldsymbol{r}\boldsymbol{r}'}| e^{i\phi_{\boldsymbol{r}\boldsymbol{r}'}}$, with a uniform distribution of amplitudes $|\chi_{\boldsymbol{r}\boldsymbol{r}'}| \in [0.02, 0.20]$ and phases $\phi_{\boldsymbol{r}\boldsymbol{r}'} \in [0, 2\pi]$. The chemical potentials are set to be the default value $\mu_{\boldsymbol{r}} = 0$ in the beginning. Obviously, the local constraints are violated here in general and the deviation of the local fermion density can be denoted as $\delta n_{\boldsymbol{r}} = 1 - \langle f^{\dagger}_{\boldsymbol{r}\alpha} f_{\boldsymbol{r}\alpha} \rangle$. The expectation value is taken using the ground state of $\mathcal{H}_{\mathrm{MF}}$ with the unchanged $\mu_{\boldsymbol{r}}$ at this stage. To obtain the correct density, one must adjust the chemical potential $\mu_{\boldsymbol{r}}$ by $\delta\mu_{\boldsymbol{r}}$ at each site. It is found that to the lowest order, the desired adjustment of chemical potentials $\delta\mu_{\boldsymbol{r}}$ can be expressed as

$$\delta\mu_{\boldsymbol{r}} = \sum_{\boldsymbol{r}'} G^{-1}(\boldsymbol{r} - \boldsymbol{r}', 0) \delta n_{\boldsymbol{r}'}, \tag{6}$$

where $G^{-1}(\boldsymbol{r} - \boldsymbol{r}', 0)$ is nothing but the inverse of the density-density correlation at zero frequency. The elements of the correlation $G(\boldsymbol{r} - \boldsymbol{r}', 0)$ can be calculated at the single-particle level from the mean-field Hamiltonian $\mathcal{H}_{\mathrm{MF}}$, with the help of the standard linear response theory in principle. However, it follows that the inversion of $G(\boldsymbol{r} - \boldsymbol{r}')$ naively diverges. Physically, this is because a uniform adjustment of the chemical potential at every site is trivial and the fermion density will remain intact. This obstacle is overcome by following the treatment suggested in Ref. [17], that is, diagonalizing $G(\boldsymbol{r} - \boldsymbol{r}', 0)$ and only focusing on its nonzero eigenvalues g_i. Note that the index i refers to the basis where $G(\boldsymbol{r} - \boldsymbol{r}', 0)$ is diagonalized. In such a basis, the relationship Eq. (6) becomes

$$\delta\mu_i = \delta n_i / g_i. \tag{7}$$

Here, the index i should not be summed. For all indices with vanishing eigenvalues g_i, μ_i is taken to be zero concurrently.

TABLE I. The SCM results of the ground and lowest competing states for $2 \leqslant N \leqslant 9$. The average background fluxes of doubled unit-cell stripe states for $N = 4$ and 5 satisfy $\phi_{\mathrm{avg}} = \pi - \pi/N$.

N	Ground state	Lowest competing state
2	dimer state	CSL $\phi = \pi/2$
3	three-site complex VCS	CSL $\phi = 2\pi/3$
4	four-site VCS	doubled unit-cell stripe
5	doubled unit-cell stripe	CSL $\phi = 4\pi/5$
$6 \leqslant N \leqslant 9$	CSL $\phi = \pi - \pi/N$	CSL $\phi = \pi - \pi/(2N)$

Then, the adjustment of the chemical potential $\delta\mu_{\boldsymbol{r}}$ is well defined. A simple replacement of $\mu_{\boldsymbol{r}} \to \mu_{\boldsymbol{r}} + \delta\mu_{\boldsymbol{r}}$ gives a new mean-field Hamiltonian $\mathcal{H}_{\mathrm{MF}}$ and related ground state. In consequence, it affects the local fermion density conversely, resulting in a new deviation $\delta n_{\boldsymbol{r}}$. These processes construct a self-consistent procedure and the problem of searching for an appropriate set of chemical potential deviation $\delta\mu_{\boldsymbol{r}}$ can be solved by iterating the procedure until the density is uniform. This is the core of the algorithm to preserve the local single-occupation constraints $n_{\boldsymbol{r}} = \langle f^{\dagger}_{\boldsymbol{r}\alpha} f_{\boldsymbol{r}\alpha} \rangle = 1$.

With the modified chemical potentials calculated in the previous step, an update set of auxiliary fields $\chi_{\boldsymbol{r}\boldsymbol{r}'}$ can be determined via $\chi'_{\boldsymbol{r}\boldsymbol{r}'} = -\mathcal{J} \langle f^{\dagger}_{\boldsymbol{r}'\alpha} f_{\boldsymbol{r}\alpha} \rangle / N$, but the local constraints may be violated once again. The amended auxiliary fields and chemical potentials can be treated as a new and better starting point. The procedure described in the previous step is thus implemented iteratively until reaching a convergence of the ground state energy within a given numerical error. It has been shown in Ref. [17] that the energy of the final state must be less than or equal to that of the initial state after the optimization process. Therefore, we eventually obtain a local energy minimum. In order to reach the global minimum as much as possible, we start from at least 50 randomly initialized fields, and reap a collection of local minima satisfying the single-occupation constraints. The lowest two are accepted as the best results of the ground state and lowest competing state energies.

IV. THE MEAN-FIELD RESULTS

We describe the ground states and lowest competing states of the mean-field Hamiltonian Eq. (4) from the SCM algorithm. Because different geometries can accommodate different candidate ground states especially cluster states with unknown dimensions, in the calculation, we consider all unit cells of a parallelogram geometry $\ell_1 \times \ell_2$ with $\ell_{1,2} \leqslant 2N$ for $2 \leqslant N \leqslant 5$ and $\ell_{1,2} \leqslant N$ for $N \geqslant 6$. In some ordered cases for $N = 4, 5$, larger unit-cell sizes are also considered for confirmation. Each unit cell is repeated by $L_{1,2}$ ($\geqslant 20$) times along the triangular Bravais lattice vectors to form a superlattice. The superlattice itself has periodic boundary conditions. In practice, for each case, we ran the SCM procedure at least 50 times with different random seeds to avoid any missing of ground states caused by numerical problems. The results are listed in Table I and Table II.

For $N = 2$ and 3, the lowest energies we found saturate the bound Eq. (5), meaning that the ground states are the dimer and three-site simplex VCS, respectively. Actually, the

TABLE II. The SCM results of the ground state and the lowest competing state energies for $2 \leqslant N \leqslant 9$. The energy is in units of $N\mathcal{J}N_s = N^2 J N_s$.

N	Ground state	Lowest competing state
2	−0.1250000	−0.1202034
3	−0.1111111	−0.0999171
4	−0.0781250	−0.0760440
5	−0.0581877	−0.0581046
6	−0.0455285	−0.0443810
7	−0.0364651	−0.0357994
8	−0.0297864	−0.0293744
9	−0.0247509	−0.0244826

obtained ground states are highly degenerate because any state with each site covered by one dimer or cluster unit has the same energy in the large-N limit. An ordered dimer or three-site simplex VCS state, as illustrated in Figs. 2(a) and 2(b), is expected to be selected beyond the mean field. Note that the nonzero expectation values $|\chi_{rr'}|$ in Figs. 1(a) and 1(b) can only take $1/2$ and $1/3$, respectively. The true ground state for $N = 2$ is the well-known 120° Néel state and differs from the mean-field here. The $N = 3$ case was also shown to have a three-sublattice magnetic order in previous numerics [27,28]. This reflects the deficiency of the large-N approximation for small-N cases. In Table I, we further find that the lowest competing states are CSL states with $\phi = \pi - \pi/N$.

The $N = 4$ case is more compelling due to the rapid growth of experimental proposals [14,15,29,30] and the large-N approximation could provide useful insight here. We find that the ground state energy does not saturate the bound Eq. (5) as excepted, but saturates the stricter bound discussed previously. The ground states are the four-site VCS depicted in Fig. 2(c), accompanied by a large degeneracy for the same reason as $N = 2$ and 3. The nonzero expectation values are $|\chi_{rr'}| = 1/4$.

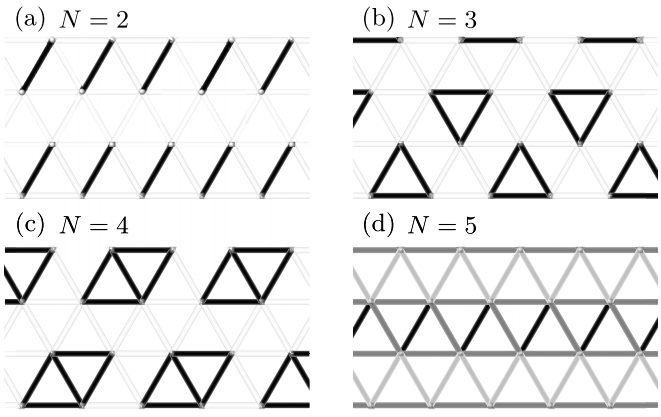

FIG. 2. Ground states in the large-N limit for (a) $N = 2$, (b) $N = 3$, (c) $N = 4$, and (d) $N = 5$. For $2 \leqslant N \leqslant 4$, any state covering all sites by the same dimer or cluster unit has the same energy in each case. We merely show one of such configurations. For $N = 5$, there is a stripe pattern with doubled unit cell along one of the lattice vectors. The grayness of bonds indicates the relative magnitude of expectation values $|\chi_{rr'}|$. Black (white) bonds refer to maximal (zero) $|\chi_{rr'}|$.

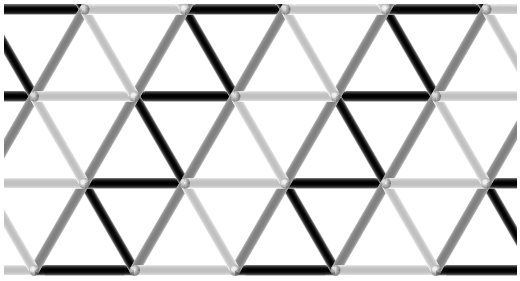

FIG. 3. The lowest competing state in the large-N limit for $N = 4$. This is a stripe pattern with doubled unit cell along one of lattice vectors. The grayness of bonds indicates the relative magnitude of expectation value $|\chi_{rr'}|$.

A similar plaquette order was also reported in a recent work [15]. In Fig. 3, we depict the lowest competing state for $N = 4$. One can see that the lattice is covered by stripes with three different bond expectation values $|\chi_{rr'}| \approx 0.030$, 0.158, and 0.224. Along one of the lattice vectors, there is a unit-cell doubling that breaks the lattice translation. The background fluxes through each plaquette are inhomogeneous as well and manifest the same unit-cell doubling pattern. Specifically, the average flux is a constant value $\phi_{\text{avg}} = \pi - \pi/N$ where $N = 4$. The same ordered pattern has also been obtained through the DMRG study from the Kugel-Khomskii model [31]. They attribute the symmetry breaking to symmetry-allowed umklapp interactions in certain finite geometries. In our results, however, such a stripy state is not the ground state even in the two-dimensional limit.

From $N = 5$, neither the bound Eq. (5) nor the stricter one can be saturated. Thus, the ground states are no longer VCS. Our numerical calculation finds that the ground state for $N = 5$ is very similar to the lowest competing state for $N = 4$ [see Fig. 2(d)], except that the bond expectation values can only take $|\chi_{rr'}| \approx 0.072$, 0.145, and 0.179, and the average background flux $\phi_{\text{avg}} = \pi - \pi/N$ shifts accordingly. It also breaks the lattice translation symmetry along one of lattice vectors and manifests itself as a stripe pattern with a doubled unit cell. The lowest competing state for $N = 5$ is a CSL with $\phi = 4\pi/5$. With further increasing N, the frustration is enhanced. Eventually, the ground states become CSL states with $\phi = \pi - \pi/N$ when $6 \leqslant N \leqslant 9$. Correspondingly, the lowest competing states we found share the identical form. They are CSL states as well except that the background magnetic fluxes shift to $\phi = \pi - \pi/(2N)$.

With the two types of CSL states identified, we now discuss the properties of these topological liquid states. The CSL is characterized by the mean-field saddle point

$$\chi_{rr'} = |\chi| e^{i a_{rr'}}, \tag{8}$$

$$\mu_r = 0. \tag{9}$$

All bonds on the lattice have a uniform expectation value for $|\chi|$ but modulated by a U(1) gauge field $a_{rr'}$ so that the flux ϕ on each plaquette is a constant. The CSL breaks both parity and time reversal. The bond phase field $a_{rr'}$ is treated as a fluctuating U(1) gauge field coupled to the fractionalized spinons. By checking the behavior of the mean-field

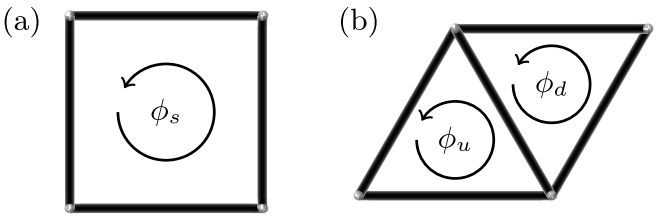

FIG. 4. The definition of the emergent U(1) gauge flux ϕ for CSL on the (a) square and (b) triangular lattices. The subscripts s, u, and d refer to the square, up-triangular, and down-triangular plaquettes, respectively.

Hamiltonian Eq. (4) at the CSL saddle points, we find that both types of CSL states have a fermion band structure with N bands where only the lowest is filled [see Fig. 1(b)]. The Fermi level lies in the gap between the lowest two bands; thus all discussion can be applied to both CSL states. Furthermore, the first type of CSL with $\phi_{u,d} = \pi - \pi/N$ on the triangular lattice can be mapped to the counterpart on a square lattice up to a time reversal. If we regard the adjacent up and down triangles as a unit shown in Fig. 4, the phase of the shared bond has no contribution to the total flux, and we have the relationship

$$\phi_u + \phi_d = -\phi_s \mod 2\pi, \tag{10}$$

where ϕ_s is the background U(1) flux through each square plaquette. In Ref. [16], Hermele *et al.* found that the CSL states are ground states for $5 \leqslant N \leqslant 10$ on the square lattice in the mean-field calculation. As the spinon is gapped out by the emergent U(1) gauge flux pattern, the Chern-Simons term enters the theory for U(1) gauge fluctuations. After integrating the gapped spinons, one obtains a topological quantum field theory with a Chern-Simons term corresponding to the chiral Abelian topological order and anyonic statistics. The spinon is converted into anyons with a statistical angle $\pi \pm \pi/N$. Gapless chiral states carrying spin degrees of freedom are also supported by the CSL as edge modes, and the low-energy theory is described by the $SU(N)_1$ WZW model.

V. DISCUSSION

To summarize, we study the Heisenberg antiferromagnets with SU(N) symmetry on the triangular lattice. In the large-N approximation, a variety of ground states and lowest competing states are identified for different parameter N. At the mean-field level, the ground state for $2 \leqslant N \leqslant 4$ is an N-site VCS state with a large degeneracy. Specifically, ordering patterns with a doubled unit cell and average background flux $\phi_{\text{avg}} = \pi - \pi/N$ are found in the $N = 4$ and 5 cases. These ordered states break the lattice translation symmetry along one of lattice vectors and become the lowest competing state and ground state for $N = 4$ and 5, respectively. The frustration from SU(N) exchange interaction is enhanced when $N > 5$, resulting in two types of CSL states as the lowest two states for $6 \leqslant N \leqslant 9$. Among them, the CSL states with $\phi = \pi - \pi/N$ have a lower energy, and have its counterpart on the square lattice. Although the true ground states are not what we found for $N < 4$, our calculation can provide useful insight for cases $N \geqslant 4$ where the large-N approximation becomes more reliable. In a very recent DMRG study of an SU(4) spin model on the triangular lattice, phase diagrams for integer fillings were obtained and compared with conventional MFT ones [15]. The quite good agreement of the phase boundaries determined by two methods suggests that $N = 4$ is perhaps large enough for the mean-field analysis we performed in this work.

Thanks to the development of ultracold experimental techniques, the SU(N) Mott insulators have been realized with AEAs on various optical lattices using the Pomeranchuk cooling [32]; even the Mott crossover and SU(N) antiferromagnetic spin correlations were recently observed with ^{173}Yb atoms [33,34]. Nontrivial physics of multicomponent fermions with broken SU(N) symmetry were also proposed on this platform [35]. The emergency of the widely concerned SU(4) or even SU(8) symmetric interaction has been proposed in the twisted bilayer graphene and double moiré layer systems recently [12,14]. This moiré lattice system could be a novel platform to detect possible phases in this work. The ultracold atom systems may have many restrictions in the detection of anyonic spinon excitations and edge states. Nevertheless, spin-dependent Bragg spectroscopy may be used to detect the spinon continuum [16–18], the singlet-triplet oscillation technique can detect the nearest-neighbor spin correlation [34] for CSLs, and the lattice potential could be adjusted to localize and manipulate the anyonic quasiparticles [16–18]. For solid-state systems, more techniques are available. These include but are not restricted to quantized thermal Hall transport [36] for the edge modes, scanning tunneling microscopy of anyons at defects [37], or even angle-resolved photon emission measurements for the spinon signatures [38].

ACKNOWLEDGMENTS

We thank Shizhong Zhang for some discussion and the proofreading of the manuscript. This work is supported by the research funds from the Ministry of Science and Technology of China with Grants No. 2016YFA0301001, No. 2018YFE0103200, and No. 2016YFA0300500, by Shanghai Municipal Science and Technology Major Project with Grant No. 2019SHZDZX04, and from the Research Grants Council of Hong Kong with General Research Fund Grants No. 17303819 and No. 17306520.

[1] A. V. Gorshkov, M. Hermele, V. Gurarie, C. Xu, P. S. Julienne, J. Ye, P. Zoller, E. Demler, M. D. Lukin, and A. M. Rey, Two-orbital SU(N) magnetism with ultracold alkaline-earth atoms, Nat. Phys. **6**, 289 (2010).

[2] C. Wu, J.-p. Hu, and S.-c. Zhang, Exact SO(5) Symmetry in the Spin-3/2 Fermionic System, Phys. Rev. Lett. **91**, 186402 (2003).

[3] C. Xu and C. Wu, Resonating plaquette phases in SU(4) Heisenberg antiferromagnet, Phys. Rev. B **77**, 134449 (2008).

[4] C. Wu, Competing Orders in One-Dimensional Spin-3/2 Fermionic Systems, Phys. Rev. Lett. **95**, 266404 (2005).

[5] C. Wu, Hidden symmetry and quantum phases in spin-3/2 cold atomic systems, Mod. Phys. Lett. B **20**, 1707 (2006).

[6] Z. Cai, H.-H. Hung, L. Wang, and C. Wu, Quantum magnetic properties of the $SU(2N)$ Hubbard model in the square lattice: A quantum Monte Carlo study, Phys. Rev. B **88**, 125108 (2013).

[7] D. Wang, Y. Li, Z. Cai, Z. Zhou, Y. Wang, and C. Wu, Competing Orders in the 2D Half-Filled SU($2N$) Hubbard Model through the Pinning-Field Quantum Monte Carlo Simulations, Phys. Rev. Lett. **112**, 156403 (2014).

[8] K. I. Kugel and D. I. Khomskii, The Jahn-Teller effect and magnetism: Transition metal compounds, Sov. Phys. Usp. **25**, 231 (1982).

[9] A. Joshi, M. Ma, F. Mila, D. N. Shi, and F. C. Zhang, Elementary excitations in magnetically ordered systems with orbital degeneracy, Phys. Rev. B **60**, 6584 (1999).

[10] W. M. H. Natori, R. Nutakki, R. G. Pereira, and E. C. Andrade, SU(4) Heisenberg model on the honeycomb lattice with exchange-frustrated perturbations: Implications for twistronics and Mott insulators, Phys. Rev. B **100**, 205131 (2019).

[11] G. Chen, R. Pereira, and L. Balents, Exotic phases induced by strong spin-orbit coupling in ordered double perovskites, Phys. Rev. B **82**, 174440 (2010).

[12] M. G. Yamada, M. Oshikawa, and G. Jackeli, Emergent SU(4) Symmetry in α-$ZrCl_3$ and Crystalline Spin-Orbital Liquids, Phys. Rev. Lett. **121**, 097201 (2018).

[13] C. Xu and L. Balents, Topological Superconductivity in Twisted Multilayer Graphene, Phys. Rev. Lett. **121**, 087001 (2018).

[14] Y.-H. Zhang and A. Vishwanath, Electrical detection of spin liquids in double moiré layers, arXiv:2005.12925.

[15] Y.-H. Zhang, D. N. Sheng, and A. Vishwanath, An $SU(4)$ chiral spin liquid and quantized dipole Hall effect in moiré bilayers, arXiv:2103.09825.

[16] M. Hermele, V. Gurarie, and A. M. Rey, Mott Insulators of Ultracold Fermionic Alkaline Earth Atoms: Underconstrained Magnetism and Chiral Spin Liquid, Phys. Rev. Lett. **103**, 135301 (2009).

[17] M. Hermele and V. Gurarie, Topological liquids and valence cluster states in two-dimensional SU(N) magnets, Phys. Rev. B **84**, 174441 (2011).

[18] G. Chen, K. R. A. Hazzard, A. M. Rey, and M. Hermele, Synthetic-gauge-field stabilization of the chiral-spin-liquid phase, Phys. Rev. A **93**, 061601(R) (2016).

[19] P. Corboz, A. M. Läuchli, K. Penc, M. Troyer, and F. Mila, Simultaneous Dimerization and SU(4) Symmetry Breaking of 4-Color Fermions on the Square Lattice, Phys. Rev. Lett. **107**, 215301 (2011).

[20] T. A. Tóth, A. M. Läuchli, F. Mila, and K. Penc, Three-Sublattice Ordering of the SU(3) Heisenberg Model of Three-Flavor Fermions on the Square and Cubic Lattices, Phys. Rev. Lett. **105**, 265301 (2010).

[21] P. Corboz, M. Lajkó, A. M. Läuchli, K. Penc, and F. Mila, Spin-Orbital Quantum Liquid on the Honeycomb Lattice, Phys. Rev. X **2**, 041013 (2012).

[22] A. Keselman, L. Savary, and L. Balents, Dimer description of the SU(4) antiferromagnet on the triangular lattice, SciPost Phys. **8**, 76 (2020).

[23] M. Hafez-Torbati, J.-H. Zheng, B. Irsigler, and W. Hofstetter, Interaction-driven topological phase transitions in fermionic SU(3) systems, Phys. Rev. B **101**, 245159 (2020).

[24] C. Boos, C. J. Ganahl, M. Lajkó, P. Nataf, A. M. Läuchli, K. Penc, K. P. Schmidt, and F. Mila, Time-reversal symmetry breaking Abelian chiral spin liquid in Mott phases of three-component fermions on the triangular lattice, Phys. Rev. Res. **2**, 023098 (2020).

[25] N. Read and S. Sachdev, Valence-Bond and Spin-Peierls Ground States of Low-Dimensional Quantum Antiferromagnets, Phys. Rev. Lett. **62**, 1694 (1989).

[26] D. S. Rokhsar, Quadratic quantum antiferromagnets in the fermionic large-N limit, Phys. Rev. B **42**, 2526 (1990).

[27] A. Läuchli, F. Mila, and K. Penc, Quadrupolar Phases of the $S = 1$ Bilinear-Biquadratic Heisenberg Model on the Triangular Lattice, Phys. Rev. Lett. **97**, 087205 (2006).

[28] B. Bauer, P. Corboz, A. M. Läuchli, L. Messio, K. Penc, M. Troyer, and F. Mila, Three-sublattice order in the SU(3) Heisenberg model on the square and triangular lattice, Phys. Rev. B **85**, 125116 (2012).

[29] P. Nataf, M. Lajkó, A. Wietek, K. Penc, F. Mila, and A. M. Läuchli, Chiral Spin Liquids in Triangular-Lattice SU(N) Fermionic Mott Insulators with Artificial Gauge Fields, Phys. Rev. Lett. **117**, 167202 (2016).

[30] H. Ozawa, S. Taie, Y. Takasu, and Y. Takahashi, Antiferromagnetic Spin Correlation of SU($\mathcal{N}$) Fermi Gas in an Optical Superlattice, Phys. Rev. Lett. **121**, 225303 (2018).

[31] A. Keselman, B. Bauer, C. Xu, and C.-M. Jian, Emergent Fermi Surface in a Triangular-Lattice SU(4) Quantum Antiferromagnet, Phys. Rev. Lett. **125**, 117202 (2020).

[32] S. Taie, R. Yamazaki, S. Sugawa, and Y. Takahashi, An SU(6) Mott insulator of an atomic Fermi gas realized by large-spin Pomeranchuk cooling, Nat. Phys. **8**, 825 (2012).

[33] C. Hofrichter, L. Riegger, F. Scazza, M. Höfer, D. R. Fernandes, I. Bloch, and S. Fölling, Direct Probing of the Mott Crossover in the SU(N) Fermi-Hubbard Model, Phys. Rev. X **6**, 021030 (2016).

[34] S. Taie, E. Ibarra-García-Padilla, N. Nishizawa, Y. Takasu, Y. Kuno, H.-T. Wei, R. T. Scalettar, K. R. A. Hazzard, and Y. Takahashi, Observation of antiferromagnetic correlations in an ultracold SU(N) Hubbard model, arXiv:2010.07730.

[35] L. Del Re and M. Capone, Selective insulators and anomalous responses in three-component fermionic gases with broken SU(3) symmetry, Phys. Rev. A **98**, 063628 (2018).

[36] Y. Gao and G. Chen, Some experimental schemes to identify quantum spin liquids, Chin. Phys. B **29**, 097501 (2020).

[37] Z. Papić, R. S. K. Mong, A. Yazdani, and M. P. Zaletel, Imaging Anyons with Scanning Tunneling Microscopy, Phys. Rev. X **8**, 011037 (2018).

[38] E. Tang, M. P. A. Fisher, and P. A. Lee, Low-energy behavior of spin-liquid electron spectral functions, Phys. Rev. B **87**, 045119 (2013).